Cooperativity transitions driven by higher-order oligomer formations in ligand-induced receptor dimerization

Masaki Watabe,[1,*] Satya N. V. Arjunan,[1,2] Wei Xiang Chew,[1,3] Kazunari Kaizu,[1] and Koichi Takahashi[1,4,5,†]

[1]*Laboratory for Biologically Inspired Computing, RIKEN Center for Biosystems Dynamics Research, Suita, Osaka 565-0874, Japan*

[2]*Lowy Cancer Research Centre, University of New South Wales, Sydney, New South Wales 2052, Australia*

[3]*Physics Department, Faculty of Science, University of Malaya, Kuala Lumpur 50603, Malaysia*

[4]*Institute for Advanced Biosciences, Keio University, Fujisawa, Kanagawa 252-8520, Japan*

[5]*Department of Biosciences and Informatics, Keio University, Yokohama, Kanagawa 223-8522, Japan*

(Received 27 May 2019; published 13 December 2019)

While cooperativity in ligand-induced receptor dimerization has been linked with receptor-receptor couplings via minimal representations of physical observables, effects arising from higher-order oligomer, e.g., trimer and tetramer, formations of unobserved receptors have received less attention. Here we propose a dimerization model of ligand-induced receptors in multivalent form representing physical observables under basis vectors of various aggregated receptor states. Our simulations of multivalent models not only reject Wofsy-Goldstein parameter conditions for cooperativity, but show that higher-order oligomer formations can shift cooperativity from positive to negative.

DOI: 10.1103/PhysRevE.100.062407

I. INTRODUCTION

Collective behavior is a phenomenon common in human, animal, cellular, and biomolecular systems. Despite varying significantly in terms of the type and composition of biological components, fundamental dynamical properties allow collectives to exhibit rapid or gradual responses in complex environments. For example, group behaviors of wild baboons have been precisely linked to characteristic S-shaped (or sigmoid) response curves via pairwise interactions of subgroups [1]. The dynamics of animal groups also exhibit parallels with collective behaviors among biomolecules in living cells, such as the process by which hemoglobin binds to oxygen [2–5]. Thus, by abstracting structural details of biomolecules and relating biochemical interactions directly to mathematical networks, we can consider key insight regarding collective behavior and likely demonstrate various aspects of biomolecular binding systems.

Collective biomolecular behavior is generally referred to as cooperativity, its main functions being to allow biomolecular binding systems to exhibit either positive or negative sigmoid responses [2–5]. For example, a conformational change in proximal and distal regions of hemoglobin complex enables efficient transport of oxygen between the lungs and tissue, exhibiting positive cooperativity: steeper sigmoid (or switch-like) responses with a threshold in a concentration range of stimuli [2–5]. Receptor systems coupling to G proteins can, however, display more gradual sigmoid curvature, achieving a less decisive but also less restricted wide concentration range of signaling molecules [2–4]. Such gradual cooperative responses are known as negative cooperativity.

In standard systems biology approaches, the fundamental rules governing cooperativity in living cells can be investigated by mapping and analyzing biomolecular networks and their parameter conditions. A key challenge of analyzing network models is finding meaningful and nonintuitive effects. Using data-driven (or inductive) modeling approaches, network models are generally constructed with various biochemical parameters, e.g., equilibrium binding constants, but restricted to observable components (or states) imposed by experimental techniques, e.g., live-cell imaging via biomolecules tagged with fluorescence emitters. The network models can lead to the parameter conditions exhibiting either positive or negative cooperativity. It is often overlooked, however, that these conditions can vary greatly by incorporating realistic but unobserved components (or states) into the network models. For example, the Monod-Wyman-Changeux model that describes allosteric regulations of proteins always exhibits positive cooperativity; nevertheless, modifications in the scale of protein's conformational changes proposed by Koshland, Nemethy, and Filmer offer parameter regions that allow negative cooperativity [2,6–8]. By introducing hidden components (or states) in the network models, cooperativity can shift from positive to negative (or negative to positive). Such cooperativity transitions thus hinder physical interpretations of the cooperativity extracted from the data-driven modeling approaches.

The collective behavior of cell-surface receptors is a key function for enabling the efficient transduction of biochemical signals to cellular interiors. Prior experimental studies have explored the origin of negative cooperativity in dimer formations for equilibrium binding of ligands to cell-surface receptors, mainly using the simplest dimerization model formulated by Wofsy and Goldstein [9–18]. While this dimerization model predicts the parameter conditions that give rise to negative cooperativity, effects arising from higher-order oligomer,

*Corresponding author: masaki@riken.jp

†Corresponding author:ktakahashi@riken.jp

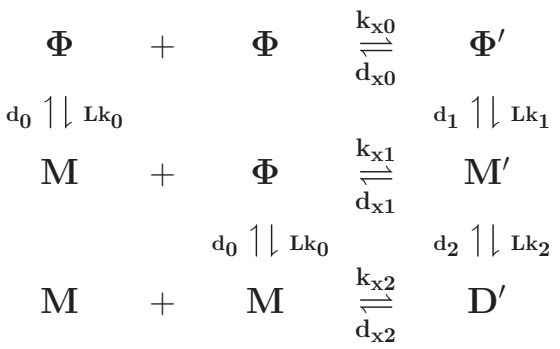

FIG. 1. Network model of observed receptor states in dimer formations. Here $\mathbf{\Phi}/\mathbf{\Phi}'$, $\mathbf{M}/\mathbf{M}'$, and $\mathbf{D}'$ are the observed receptor-state vectors in the formation of nulls, monomers, and dimers, respectively. Each observed receptor state is represented under basis vectors of various aggregated receptor states. Here $\mathbf{k_i}$ and $\mathbf{d_i}$ are the association and dissociation rates of the ith index, respectively; $\mathbf{L}$ is the ligand concentration.

e.g., trimer and tetramer, formations of unobserved receptors have received less attention. In this article, we consider dimerization models in multivalent form that represent physical observables under basis vectors of various aggregated receptor states (see Fig. 1). We then evaluate the cooperative behavior that arises from multivalent models, comparing it with the cooperativity expected from the Wofsy-Goldstein (WG) formulation. Our results from model simulations imply violation of the WG parameter conditions. We also demonstrate how a mixture of various aggregated receptor states in the multivalent models can lead to the transition of cooperativity from positive to negative.

II. THEORETICAL FRAMEWORK

We consider the following assumptions: (a) There is no internalization of ligands and receptors, (b) each binding process is independent of chain and ring formation, (c) the four local equilibrium constants (K_{x0}, K_0, K_1, and K_2) are dependent on each other, and (d) detailed balance conditions are given by $K_{x1} = K_{x0}K_1/K_0$ and $K_{x2} = K_{x0}K_1K_2/K_0^2$.

In the state-vector representation of physical observables, the dimerization model is described by a function containing the probabilities of biochemical interactions that form various aggregated receptor states. All possible aggregated receptor states in the dimerization models can be treated mathematically as basis vectors in a multidimensional real vector space. The receptor-state vectors observed in the formation of nulls ($\mathbf{\Phi}$ and $\mathbf{\Phi}'$), monomers ($\mathbf{M}$ and $\mathbf{M}'$), and dimers ($\mathbf{D}'$) are given by

$$\mathbf{\Phi} = \begin{pmatrix} r \\ rr \\ rrr \\ \vdots \\ r^N \end{pmatrix}, \quad \mathbf{M} = \begin{pmatrix} R \\ Rr \\ Rrr \\ \vdots \\ Rr^{N-1} \end{pmatrix}, \quad \mathbf{\Phi}' = \begin{pmatrix} r \cdot r \\ r \cdot rr \\ r \cdot rrr \\ \vdots \\ r^N \cdot r^N \end{pmatrix},$$

$$\mathbf{M}' = \begin{pmatrix} R \cdot r \\ R \cdot rr \\ R \cdot rrr \\ \vdots \\ Rr^{N-1} \cdot r^N \end{pmatrix}, \quad \mathbf{D}' = \begin{pmatrix} R \cdot R \\ R \cdot Rr \\ R \cdot Rrr \\ \vdots \\ Rr^{N-1} \cdot Rr^{N-1} \end{pmatrix}, \tag{1}$$

where r and R represent the receptors and the ligand-mediated receptors, respectively, and N is the number of receptors that can be aggregated in the $\mathbf{\Phi}$ and $\mathbf{M}$ observed states. There are N^2 elements in the $\mathbf{\Phi}'$, $\mathbf{M}'$, and $\mathbf{D}'$ observed states.

Figure 1 shows a network of observed receptor states in the dimerization model. In first-order interactions of ligands with receptors, the rates of association ($\mathbf{k_0}$, $\mathbf{k_1}$, and $\mathbf{k_2}$) and dissociation ($\mathbf{d_0}$, $\mathbf{d_1}$, and $\mathbf{d_2}$) are represented by $N \times N$ and/or $N^2 \times N^2$ diagonal matrices acting upon the basis vectors, transforming one aggregated state to one observed state.

The dissociation rates ($\mathbf{d_{x0}}$, $\mathbf{d_{x1}}$, and $\mathbf{d_{x2}}$) for the receptor-receptor interactions are represented by $N^2 \times N^2$ diagonal matrices. Nondiagonal matrices of the association rates can however transform into a mixture of various aggregated states in one observed state. The nondiagonal matrices can be written in the form

$$\mathbf{k_{x0}} = k_{x0}\mathbf{F_{x0}}, \quad \mathbf{k_{x1}} = k_{x1}\mathbf{F_{x1}}, \quad \mathbf{k_{x2}} = k_{x2}\mathbf{F_{x2}}, \tag{2}$$

where k_{xi} and $\mathbf{F_{xi}}$ are the receptor-receptor association rate and $N \times N$ scaling matrices of the ith index, respectively.

For convenience, we redefine the dimensionless lumped parameter that constrains the fraction of dimer formations in the absence of ligands. The lumped parameter can be rewritten in the matrix form

$$\mathbf{k_x} = k_x\mathbf{F_{x0}}, \tag{3}$$

where k_x is the dimensionless lumped parameter originally defined in the WG formulations [9].

III. MULTIVALENT MODELS

We construct monovalent ($N = 1$) and bivalent ($N = 2$) cell models of ligand-induced receptor dimerization. We then use the E-Cell platform [19,20] to simulate the cell models of biological fluctuation that arise from stochastic changes in the cell-surface geometry, number of receptors, ligand binding, molecular states, and diffusion constants. These cell models assume that the nondiffusive receptors are uniformly distributed on a flat cell surface measuring 100 and 100 μm on the horizontal and vertical axes, respectively. We also assume that the total receptor concentration, binding affinity, and dissociation rates for each interaction are given by $T = 4.977$ receptors/μm^2, $K_0 = 1.00$ nM, $d_0 = 0.01$ s^{-1}, $d_1 = 10^{-5}$ s^{-1}, $d_2 = 1.00$ s^{-1}, and $d_{x0} = d_{x1} = d_{x2} = 1.00$ s^{-1}. The relation of the local equilibrium constants to the association and dissociation rates is also given by $K_i = d_i/k_i$, where $i = 0, 1, 2, x0, x1, x2$. In a concentration range of ligand stimuli from 10^{-4} to 100 nM, we run model simulations for a period of 100 000 s to verify the complete convergence of receptor response to full equilibrium.

The scaling factor and matrices in the monovalent model are given by $k_x = T/K_{x0}$ and $\mathbf{F_{x0}} = \mathbf{F_{x1}} = \mathbf{F_{x2}} = \alpha$. In the

bivalent model, we assume that the symmetric scaling matrices can be written in the form

$$\mathbf{F_{x0}} = \mathbf{F_{x1}} = \begin{pmatrix} \alpha & \gamma\sqrt{\alpha\beta} \\ \gamma\sqrt{\alpha\beta} & \beta \end{pmatrix}, \quad \mathbf{F_{x2}} = \begin{pmatrix} \alpha & 0 \\ 0 & 0 \end{pmatrix}, \quad (4)$$

where α, β, and γ are matrix elements; γ must be less than unity to satisfy the positive-definite condition. The second-order interactions forming oligomers, e.g., dimers and trimers, in the null and monomeric observables are given by

$$\mathbf{\Phi}^{\dagger}\mathbf{k_{x0}}\mathbf{\Phi}, \quad (5)$$

$$\mathbf{M}^{\dagger}\mathbf{k_{x1}}\mathbf{\Phi}, \quad (6)$$

where $\mathbf{\Phi}^{\dagger}$ and $\mathbf{M}^{\dagger}$ represent dual vectors of the null and monomeric observables, respectively. In these formulations, the second-order interaction of the null observables can exhibit null dimers, trimers, and tetramers: $r + r \rightarrow rr$, $r + rr \rightarrow rrr$, and $rr + rr \rightarrow rrrr$. Monomeric dimers, trimers, and tetramers can be formed also through the second-order interactions between the null and monomeric observables: $R + r \rightarrow Rr$, $rR + r \rightarrow rRr$, $R + rr \rightarrow Rrr$, and $rR + rr \rightarrow rRrr$. There are no dimeric trimers and tetramers defined in the bivalent model.

IV. THE WG FORMULATION

The network diagram of the WG dimerization model is equivalent to that of the monovalent model. The dimerization process was however formulated under a "special" assumption that the local equilibrium constant of a direct receptor-receptor (or second-order) interaction (K_{x0}) is independent of first-order interactions of receptors associated with ligands (K_0, K_1, and K_2). The total cell-surface receptor concentrations and the number of ligand-induced oligomers per a unit surface area are given by

$$T = (1 + LK_0)X + K_{x0}(1 + 2LK_1 + L^2K_1K_2)X^2, \quad (7)$$

$$B = LK_0X + K_{x0}\left(LK_1 + \tfrac{1}{2}L^2K_1K_2\right)X^2, \quad (8)$$

where X and L are the concentration of unbound receptors and ligand concentration input in nM, respectively. The $\frac{1}{2}$ factor in the third term of Eq. (8) is meant to count the dimers as single molecules. Unit representations of local equilibrium constants in this formulation are not consistent with the units in our multivalent formulation, thereby requiring a unit transformation $K_i \rightarrow K_i^{-1}$, where $i = 0, 1, 2, x0$.

This WG formulation leads to a parameter condition that approximately exhibits negative cooperativity. The condition can be written in the form

$$\frac{K_1(K_1 - K_2)}{(K_1 - K_0)^2} \geqslant \frac{\sqrt{1 + 4k_x} - 1}{2k_x\sqrt{1 + 4k_x}}, \quad (9)$$

where k_x ($=TK_{x0}$) is the dimensionless lumped parameter. This relation implies that the model always exhibits positive cooperativity if $K_1 = K_2$.

V. MODEL COMPARISON

Cooperative effects can be generally seen in the concavity of the Scatchard plots. We compare the Scatchard plots among the three cell models configured to have the same parameter values. Model differences can be clearly seen in Figs. 2(b), 2(d), and 2(f). For $k_x = 0.01$ and 0.10, the Scatchard plots of the three models exhibit concave downward curvatures that approximately represent positive cooperativity. The bivalent model ($k_x = 0.30$) in Fig. 2(f), however, exhibits a concave-up curve of the Scatchard plot that represents negative cooperativity. If the Scatchard plot represents a straight line, then there is no cooperativity. These comparison results thus imply that cooperative effects can vary as a function of the lumped parameter k_x.

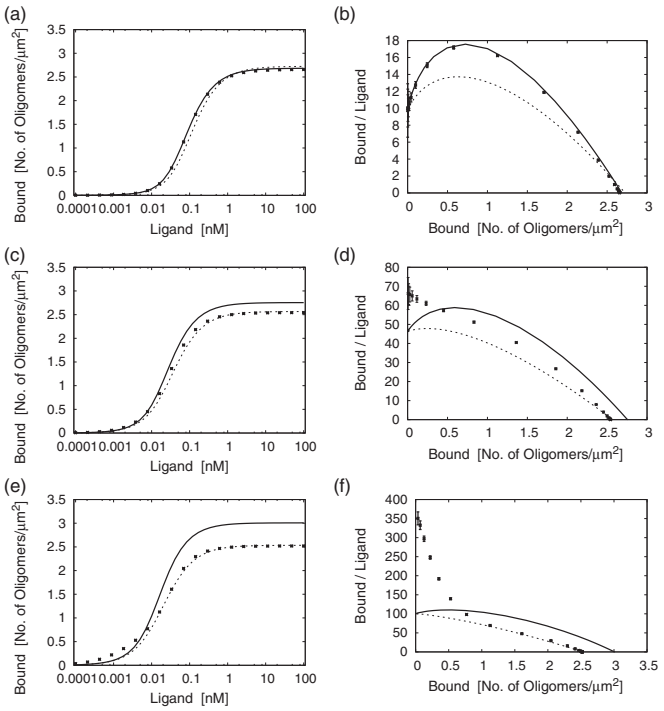

FIG. 2. Model comparison. We compare the binding curves and Scatchard plots among the three models assuming $K_1 = K_2 = 100K_0$: the WG formulation, monovalent model ($\alpha = 1$), and bivalent model ($\alpha = \beta = 1$ and $\gamma = 0$), for (a) and (b) $k_x = 0.01$, (c) and (d) $k_x = 0.10$, and (e) and (f) $k_x = 0.30$. The black solid and dashed lines represent the response curves for the monovalent model and the WG formulation, respectively. Black crosses represent the bivalent model.

Cooperative effects can be seen also in the shape of the equilibrium binding curves. We compare the binding curves among the three cell models configured to have the same parameter values. For $k_x = 0.01$, 0.10, and 0.30, the comparison results are shown in Figs. 2(a), 2(c), and 2(e), respectively. In standard systems biology approaches, the Hill function can be fitted to the binding curves to quantify the cooperative characteristics in the cell models. The Hill function can generally be written in the form of

$$B(L) = \frac{B_0L^n}{K_A^n + L^n}, \quad (10)$$

where L, B_0, K_A, and n represent the ligand concentration, maximum area density of the ligand-induced oligomers, ligands occupying half of the oligomers, and the Hill coefficient, respectively. If the Hill coefficient is less than unity ($n < 1$),

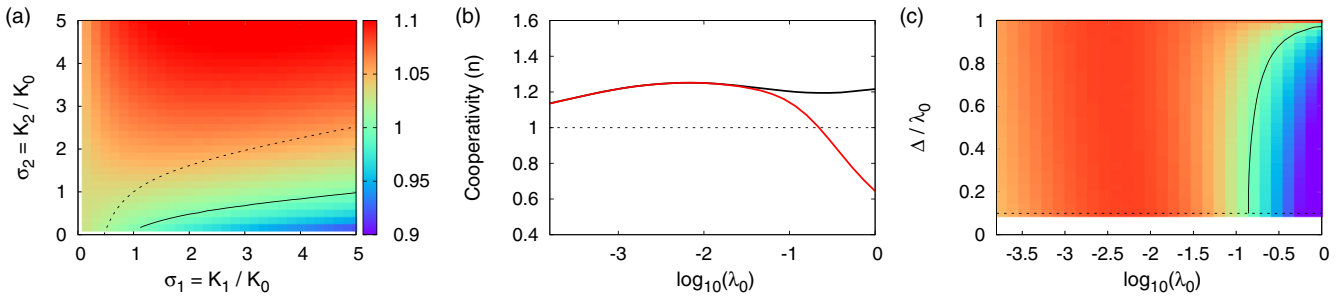

FIG. 3. Cooperativity of monovalent and bivalent models. (a) Cooperativity of the monovalent model is shown as a function of the first and second ligand-receptor equilibrium constants, assuming $k_x = 0.10$. Colors represent cooperativity n of the monovalent model. The black solid and dashed lines represent no cooperativity ($n = 1$) in the monovalent model and the WG condition given by Eq. (9), respectively. (b) and (c) Cooperativity of the bivalent model shown as a function of the eigenvalues, assuming $K_1 = K_2 = 100K_0$ and $k_x = 0.01$. Here α is varied from 0.01 to 100. (b) $\lambda_+ = \lambda_-$ ($\gamma = \Delta = 0.00$). The black and red solid lines represent cooperativity of the monovalent and bivalent models as a function of λ_0, respectively. The black dashed line corresponds to no cooperativity ($n = 1$). (c) $\lambda_+ \neq \lambda_-$ ($\gamma = 0.10$). The black line represents no cooperativity. Colors represent cooperativity n in the range from 0.7 (blue) to 1.3 (red). The black dashed line is the physical limit to satisfy the positive-definite condition.

then the receptor system exhibits negative cooperativity. If $n > 1$, then cooperativity is positive. There is no cooperativity if $n = 1$.

For a fixed $k_x = 0.10$, the best-fit Hill coefficients of the monovalent model are mapped as a function of K_1 and K_2. In Fig. 3(a) the cooperativity mapping result is shown and compared with the WG condition given by Eq. (9). This comparison result clearly shows suppression of the negative cooperative region in the monovalent model, implying inconsistent cooperative responses between the monovalent model and the WG formulation.

VI. DIAGONALIZATION

To see the cooperative effects that arise from the second-order interactions forming the higher-order oligomers in the bivalent model [see Eqs. (5) and (6)], we diagonalize the lumped parameter matrix $\mathbf{k_x}$. Eigenvalues are given by

$$\lambda_\pm = \frac{k_x}{2}[(\alpha+\beta) \pm \sqrt{(\alpha-\beta)^2 + 4\gamma^2\alpha\beta}] = \lambda_0 \pm \Delta, \tag{11}$$

where the dynamic range is $\gamma\lambda_0 \leqslant \Delta \leqslant \lambda_0$.

We compare cooperative responses between the monovalent and bivalent models when the eigenvalues of the lumped parameter matrix in the bivalent model are identical ($\lambda_+ = \lambda_-$). Figure 3(b) shows the cooperativity transition of the bivalent model as a function of the λ_0 component in Eq. (11). While cooperativity is always positive in the monovalent model (black line), cooperativity in the bivalent model is shifted from positive to negative through the increase of λ_0 (red line). In the lower-λ_0 range, the second-order couplings are weakly linked with cooperative responses, displaying identical cooperativity between the monovalent and bivalent models. The higher-λ_0 values in the bivalent model, however, can increase the event number of trimers (rrR) and tetramers ($rrrR$) in the monomeric observable $\mathbf{M}'$. Also, these higher-order oligomers are weakly linked with the first-order couplings that represent ligand dissociation ($rrR \rightarrow rrr$ and $rrrR \rightarrow rrrr$) and association ($rrR \rightarrow rRR$ and $rrrR \rightarrow rrRR$). Because of these model parameter relations, the bivalent model exhibits the transition of cooperativity in the higher-λ_0 range.

We also evaluate cooperative responses in the bivalent model in the case of differing eigenvalues ($\lambda_+ \neq \lambda_-$). Figure 3(c) shows cooperativity of the bivalent model as a function of the λ_0 and Δ components in Eq. (11). As the ratio of these components converges to unity $\Delta/\lambda_0 \rightarrow 1$ (or $\beta \rightarrow 0$), the bivalent model becomes equivalent to the monovalent model, exhibiting positive cooperativity in the full λ_0 range. While cooperativity is always positive at $\Delta/\lambda_0 = 1$ (or $\beta = 0$), the trimer and tetramer formations in the monomeric observable can change cooperativity from positive (red region) to negative (blue region) for $\Delta/\lambda_0 < 1$ (or $\beta > 0$).

Our results may have biophysical implications in data-driven modeling approaches. Many biomolecular binding processes have been modeled under the scenario that the second-order couplings are weakly linked with cooperative effects. For example, the dimerization model that describes heregulin (HRG) binding with ErbB receptors in living cells was constructed using fluorescence microscopy images via HRG tagged with tetramethylrhodamine [18]. In this model, the first-order coupling representing a conformational change of the receptor complex in the monomeric observable ($rR \leftrightarrow r'R$) plays a key role that gives rise to negative cooperativity. Nevertheless, there exist various aggregated receptor states hidden in the physical observables. These states are realistic but unobserved through the fluorescent imaging techniques. By incorporating the second-order interactions forming higher-order oligomers that can include unobserved receptors into the dimerization model, cooperativity may shift from positive to negative and vice versa. Because of these transitions, the data-driven modeling approach is not a straightforward method to identify physical sources giving rise to negative cooperative effects in the receptor systems.

VII. CONCLUSION

In this article, we explored the origin of negative cooperativity in dimer formations for equilibrium binding of ligands

to cell-surface receptors, in terms of biochemical parameters for associations and dissociations. While receptor-receptor couplings in the ligand-induced receptor dimerization have been linked previously with cooperativity via minimal representations of physical observables, cooperative effects that arise from the mixture of various aggregated receptor states hidden in each observed receptor state have received less attention. In particular, we examined the cooperativity of monovalent and bivalent models. Our results from model simulations showed the suppression of negative cooperative regions in the monovalent model, thereby implying violation of parameter conditions expected from the WG formulation. We also demonstrated that the presence of higher-order oligomer formations in the bivalent model leads to the transition of cooperativity from positive to negative, thus affecting physical interpretations of the cooperativity extracted from data-driven modeling approaches. Furthermore, it is interesting to extend our state-vector representations to more general model frameworks by incorporating heterodimer formations of receptor-family members, e.g., dimerization of ErbB3 and EGF receptors [21,22].

ACKNOWLEDGMENTS

We would like to thank Yasushi Okada, Tomonobu M. Watanabe, Jun Kozuka, Michio Hiroshima, Kozo Nishida, Suguru Kato, Toru Niina, Koji Ochiai, Keiko Itano, Kotone Itaya, and Kaoru Ikegami for their guidance and support throughout this research. We would also like to thank Kylius Wilkins for a critical reading of the manuscript. This research work was supported by JSPS (Japanese Society for the Promotion of Science) KAKENHI Grant No. 15K12146.

[1] A. Strandburg-Peshkin, D. R. Farine, M. C. Crofoot, and I. D. Couzin, Habitat and social factors shape individual decisions and emergent group structure during baboon collective movement, eLife **6**, e19505 (2017); A. Strandburg-Peshkin, D. R. Farine, I. D. Couzin, and M. C. Crofoot, Shared decision-making drives collective movement in wild baboons, Science **348**, 1358 (2015).

[2] D. E. Koshland and K. Hamadani, Proteomics and models for enzyme cooperativity, J. Biol. Chem. **277**, 46841 (2002).

[3] J. E. Ferrell, Q&A: Cooperativity, J. Biol. **8**, 53 (2009).

[4] M. I. Stefan and N. L. Nove, Cooperative binding, PLoS Comput. Biol. **9**, e1003106 (2013).

[5] R. Phillips, J. Kondev, J. Theriot, H. G. Garcia, and Orme, *Physical Biology of the Cell*, 2nd ed. (Garland Science, New York, 2013).

[6] J. Monod, J. Wyman, and J. P. Changeux, On the nature of allosteric transitions: A plausible model, J. Mol. Biol. **12**, 88 (1965).

[7] D. E. J. Koshland, D. Nemethy, and G. Filmer, Comparison of experimental binding data and theoretical models in proteins containing subunits, Biochemistry **5**, 365 (1966).

[8] F. Alan, *Structure and Mechanism in Protein Science: A Guide to Enzyme Catalysis and Protein Folding*, 1st ed. (Freeman, New York, 1999).

[9] C. Wofsy, B. Goldstein, K. Lund, and H. S. Wiley, Implications of epidermal growth factor (EGF) induced egf receptor aggregation, Biophys. J. **63**, 98 (1992); C. Wofsy and B. Goldstein, Interpretation of Scatchard plots for aggregating receptor systems, Math. Biosci. **112**, 115 (1992).

[10] P. Klein, D. Mattoon, M. A. Lemmon, and J. Schlessinger, A structure-based model for ligand binding and dimerization of EGF receptors, Proc. Natl. Acad. Sci. USA **101**, 929 (2004).

[11] K. Mayawala, D. G. Vlachos, and J. S. Edwards, Computational modeling reveals molecular details of epidermal growth factor binding, BMC Cell Biol. **6**, 41 (2005).

[12] K. Mayawala, D. G. Vlachos, and J. S. Edwards, Heterogeneities in EGF receptor density at the cell surface can lead to concave up Scatchard plot of EGF binding, FEBS Lett. **579**, 3043 (2005).

[13] F. Özcan, P. Klein, M. A. Lemmon, I. Lax, and J. Schlessinger, On the nature of low- and high-affinity EGF receptors on living cells, Proc. Natl. Acad. Sci. USA **103**, 5735 (2006).

[14] J. L. Macdonald and L. J. Pike, Heterogeneity in EGF-binding affinities arises from negative cooperativity in an aggregating system, Proc. Natl. Acad. Sci. USA **105**, 112 (2008).

[15] M. A. Lemmon, Ligand-induced ErbB receptor dimerization, Exp. Cell Res. **315**, 638 (2008).

[16] S. Adak, D. DeAndrade, and L. J. Pike, The tethering arm of the EGF receptor is required for negative cooperativity and signal transduction, J. Biol. Chem. **286**, 1545 (2011).

[17] L. Pike, Negative co-operativity in the EGF receptor, Biochem. Soc. Trans. **40**, 15 (2012).

[18] M. Hiroshima, Y. Saeki, M. Okada-Hatakeyama, and Y. Sako, Dynamically varying interactions between heregulin and ErbB proteins detected by single-molecule analysis in living cells, Proc. Natl. Acad. Sci. USA **109**, 13984 (2012); M. Hiroshima and Y. Sako, Regulation mechanism of ErbB-heregulin interaction shown by single-molecule kinetic analysis in living cells, Biophys. Physicobiol. **53**, 317 (2013).

[19] M. Tomita, K. Hashimoto, K. Takahashi, T. Shimizu, Y. Matsuzaki, F. Miyoshi, K. Saito, S. Tanida, K. Yugi, and J. Venter, E-CELL: Software environment for whole-cell simulation, Bioinformatics **15**, 72 (1999).

[20] S. N. V. Arjunan and M. Tomita, A new multicompartmental reaction-diffusion modeling method links transient membrane attachment of *E. coli* MinE to E-ring formation, Syst. Synth. Biol. **4**, 35 (2010).

[21] K. Itano, T. Ito, S. Kawasaki, Y. Murakami, and T. Suzuki, Mathematical modeling and analysis of ErbB3 and EGFR dimerization process for the gefitinib resistance, JSIM Lett. **10**, 33 (2018).

[22] T. Ito, Y. Kumagai, K. Itano, T. Maruyama, K. Tamura, S. Kawasaki, T. Suzuki, and Y. Murakami, Mathematical analysis of getfitinib resistance of lung adenocarcinoma caused by MET amplification, Biochem. Biophys. Res. Commun. **511**, 544 (2019).